Model-Based Control Strategies to Enhance Energy Flexibility in Electrically Heated School Buildings

Navid Morovat [1,*], Andreas K. Athienitis [1], José Agustín Candanedo [1,2] and Benoit Delcroix [3]

1   Center for Zero-Energy Building Studies, Concordia University, Montreal, QC H3G 1M8, Canada; andreask.athienitis@concordia.ca (A.K.A.); jose.candanedoibarra@canada.ca (J.A.C.)
2   CanmetENERGY, Natural Resources Canada, Varennes, QC J3X 1P7, Canada
3   Laboratoire des Technologies de l'Énergie, Hydro-Québec Research Institute, Shawinigan, QC G9N 0C5, Canada; delcroix.benoit@hydroquebec.com
*   Correspondence: n_morova@encs.concordia.ca

Abstract: This paper presents a general methodology to model and activate the energy flexibility of electrically heated school buildings. The proposed methodology is based on the use of archetypes of resistance–capacitance thermal networks for representative thermal zones calibrated with measured data. Using these models, predictive control strategies are investigated with the aim of reducing peak demand in response to grid requirements and incentives. A key aim is to evaluate the potential of shifting electricity use in different archetype zones from on-peak hours to off-peak grid periods. Key performance indicators are applied to quantify the energy flexibility at the zone level and the school building level. The proposed methodology has been implemented in an electrically heated school building located in Québec, Canada. This school has several features (geothermal heat pumps, hydronic radiant floors, and energy storage) that make it ideal for the purpose of this study. The study shows that with proper control strategies through a rule-based approach with near-optimal setpoint profiles, the building's average power demand can be reduced by 40% to 65% during on-peak hours compared to a typical profile.

Keywords: energy flexibility; model-based control strategies; school buildings; measured data

1. Introduction

Electric utilities consider demand-side management (DSM) a key solution to reduce peak power demand. In periods of peak power demand, using DSM is more cost-effective than operating peaking power plants or purchasing power from other jurisdictions [1]. DSM can have an even more significant effect on the grid when integrated with renewable energy sources (RESs). Buildings are important components of smart electricity grids; they can provide flexible services to reduce peak loads and shift demand in accordance with local RES production, such as energy storage in thermal mass and batteries [2,3], charging of electric vehicles [4], and HVAC system adjustments [5]. Ruilova et al. [6] defined energy flexibility in buildings as "the possibility to deviate the electricity consumption of a building from the reference scenario at a specific point in time and during a certain period". Annex 67 of the IEA Energy in Buildings and Communities Programme (IEA-EBC) defined energy flexible buildings as those with "the ability to manage [their] demand and generation according to local climate conditions, user needs, and grid requirements" [5]. Energy flexibility takes into consideration two-way communications between buildings and the power grid. In this way, buildings are regarded not as consumers but as prosumers [7]. Energy flexibility can be referred to in two ways: thermal energy storage and shifting equipment operation. According to the first approach, the energy consumption of a specific electrical device can be predicted based on the thermal properties of the device or building to minimize electricity consumption. In the second approach, some electrical devices can be controlled to shift the electricity demand to periods with lower electricity prices or

greater renewable energy generation [8]. Based on the published literature and presented in IEA-EBC Annex 67, increasing energy flexibility for the design of smart energy systems and buildings is influenced by (1) physical features of the building [2,3], (2) heating, ventilation, and air conditioning (HVAC) systems [5], (3) appropriate control systems and strategies [5], and (4) IEQ requirements [9]. In this context, an effective application of control strategies within HVAC systems is essential for increasing buildings' efficiency [10–12] and energy flexibility [13].

Finck et al. [14] developed a method and tested it under real-life conditions, including the stochastic behavior of occupants and the dynamic behavior of the building and heating system. They used key performance indicators to quantify energy flexibility by considering: (1) energy and power, (2) energy efficiency, and (3) energy costs. They found that this categorization helps to make clear the benefits of using flexibility indicators in real-life applications. Junker et al. [15] presented a methodology for evaluating energy flexibility based on the flexibility function, to describe how a particular smart building or cluster of smart buildings reacts to a penalty signal. Coninck and Helsen [16] developed a methodology to quantify flexibility in buildings based on the cost curve. The methodology returns the amount of energy that can be shifted and the costs of this load shifting. Tauminia et al. [17] proposed a multidisciplinary approach to finding trade-offs between the need to limit environmental impacts and the trend toward higher building energy performance. They found that an oversized photovoltaic (PV) system is not the best solution for load-matching, grid interactions, and environmental impacts in the absence of storage systems. They noted that installing a storage system in conjunction with the appropriate size of a PV system would result in an improved load-matching of the building and reduce grid dependence at low generation times.

Montreal (Québec, Canada) is categorized in climate zone 6 [18], meaning it experiences extreme cold weather during winter. Québec generates most of its electricity (99.8%) from hydroelectric plants, and most commercial buildings rely on electricity as their primary or only energy source [19]. Thus, during cold weather in Québec, the morning peak load (6:00 a.m. to 9:00 a.m.) and evening peak load (4:00 p.m. to 8:00 p.m.) put a strain on the electrical grid [20]. Thus, it is imperative to analyze energy consumption and develop control strategies that effectively reduce and shift peak electricity demand due to heating in buildings. In this context, obtaining a model that provides reliable predictions and can be implemented in real controllers is crucial for optimizing building performance.

The Québec province has over 2600 schools, reaching over 1 million students and almost 100,000 teachers and other staff [21]. Therefore, quantification of energy flexibility in school buildings has a significant role in providing a safe and efficient operation of the future resilient grid. Additionally, indoor environmental quality (IEQ) has a considerable impact on the health and well-being of teachers and students. Thus, simultaneously meeting the need to improve energy flexibility as a grid requirement and the growing demands for environmental performance (especially during/after the COVID pandemic) is of utmost importance to be considered. To achieve these goals, we need to develop models for a school building that provide reliable predictions and can be generalized for widespread deployment in schools.

Although school buildings contribute considerably to the total energy needs, few studies have been focused on school buildings in Canada [22,23]. They examined the energy use intensity (EUI) of 129 elementary and junior high schools in Manitoba, Canada, using data collected from 30 school buildings over ten years. They found that the average EUI at a K-12 school is 127 kWh/m^2/year, 264 kWh/m^2/year at a junior high school, and 270 kWh/m^2/year at an elementary school. They stated that energy consumption might differ between K-12 and elementary and secondary schools due to differences in equipment and activities. Another study by Ouf et al. [23] examined the use of electricity and natural gas in Canadian schools. They divided the schools into three categories based on the year they were built: before 2004, between 2004 and 2013, and after 2013. They found that the electricity EUIs before 2004 was 58 kWh/m^2/year, between 2004 and 2013

was 116 kWh/m^2/year, and after 2013 was 125 kWh/m^2/year. Newly constructed schools are more energy efficient in heating and cooling, but school electricity usage has increased due to the electrification of heating systems and additional teaching equipment.

Building energy performance simulation (e.g., EnergyPlus^{TM} and TRNSYS) is a popular approach to studying school buildings. However, studies based on control-oriented models and measured sensor data of schools are relatively rare. This study investigates measured field data in an archetype electrically heated school building in cold regions. The main objectives of this paper are to: (1) develop a methodology to create data-driven control-oriented models that facilitate developing and assessing the impact of alternative control strategies in the schools; (2) propose different control strategies aimed to enhance the energy flexibility potential of school buildings; and (3) introduce key performance indicators (KPIs) as key parameters to quantify energy flexibility at the zone and building levels while considering IEQ.

2. Methodology

In recent years, international initiatives have recognized the need for a methodology to assess energy flexibility in buildings. This paper outlines the following steps in the method:

1. Identification of the system and load.
2. Characterization of flexibility.
3. Analyzing the impact of scenario modeling on the demand profiles.
4. Proposing key performance indicators to facilitate interaction between building operators, aggregators, and utility companies.

In addition, the method should be scalable and easy to implement [24]. Following these steps, this paper aims to model and enhance the energy flexibility of electrically heated school buildings through a rule-based approach with near-optimal setpoint profiles based on the archetype grey-box models. These archetype models can be adjusted depending on the specific features of the building. This study presents a practical methodology that facilitates the modeling and widespread implementation of appropriate control strategies in school buildings.

2.1. Data-Driven Grey-Box Model

Data-driven grey-box models ensure both physical insight and the reliability of measured data. Literature review indicates that grey-box models are also suitable for demand-side management in smart grids [25–28]. Gouda and Danaher [25] proposed a second-order model in which each construction element is modeled using three resistances and two capacitances. Candanedo and Dehkordi [26] presented a generalized approach for creating reduced-order control-oriented models. Their methodology can be implemented in building simulation tools to generate simplified models automatically. Bacher and Madsen [27] developed a statistical method for identifying models in building thermal studies. Reynders et al. [28] analyzed two detached single-family houses in Belgium. These two buildings represent two extreme cases of detached single-family houses in Belgium regarding insulation level (high and low insulation levels). They used data obtained from detailed building simulations with the IDEAS library in Modelica software. This study investigated five grey-box model types, ranging from first- to fifth-order models.

In grey-box models, choosing an appropriate level of resolution is essential, as it directly affects the parameter tuning and calculation time. A high-order model containing too many parameters requires information that is not often available with adequate accuracy. An oversimplified model may not be accurate enough to help make decisions. Therefore, obtaining a model that provides reliable predictions and can be implemented in real controllers is crucial for optimal building performance.

This paper investigates the accuracy of data-driven grey-box models for energy demand simulation and energy flexibility analysis. Providing a closer link between smart grids and smart buildings requires appropriate control strategies. Thus, this study presents an application of the developed model for control purposes based on smart grid re-

quirements. The following steps are used to develop grey-box models and quantify energy flexibility:

1. Real building measurement data are collected from the smart meters installed in the archetype zones. Data included variables such as electricity consumption (kW), zone air temperature (°C), weather data, and specific data are related to each zone (e.g., floor heating temperature). All measurements are taken at intervals of 15 min.
2. Numerical models of thermal building control are developed. These models are based on RC model thermal networks.
3. The developed models are calibrated using the collected data. The important parameters are identified using the Sequential Least-Squares Programming (SLSQP) in Python.
4. Appropriate control strategies for zones with the convective system are presented to enhance the energy flexibility available from the building to the grid at specific times, depending on the grid requirement.
5. A building energy flexibility index (BEFI) is applied to quantify dynamic building energy flexibility at the zone and building levels.
6. Predictive control strategies for zones with the convective system and hydronic radiant floor system are presented to use the maximum thermal capacity of the concrete slab, reduce peak load during on-peak hours, and enhance energy flexibility when needed by the grid.

2.2. Governing Equation

A fully explicit finite difference approach is used to solve the energy balance equations at each node in the models. The fully explicit approach assumes that the current temperature of a given node depends only on its temperature and the temperature of the surrounding nodes at a previous time step. By using the heat balance for the control volume, a node's differential equation can be written as [29]:

$$T_i^{t+1} = \frac{\Delta t}{C_i}\left[\sum_j U_{ij}^t(T_j^t - T_i^t) + \sum_k U_{ik}^t(T_k^t - T_i^t) + \dot{Q}_i^t\right] + T_i^t \tag{1}$$

- U_{ij}: Thermal conductance between nodes i and j, W/K;
- U_{ik}: Thermal conductance between nodes i and k that node k has a known temperature, W/K.
- T: Temperature at node i, °C.
- C_i: Thermal capacitance at node i J/K.
- $\dot{Q}$: Heat source at node i, W.
- Δt: Time step, s.

The capacitance of the air node contains a factor C_T (air thermal capacitance multiplier) that accounts for phenomena such as (energy storage in furniture and objects, the time required for air mixing, delay due to ducting and other factors) that in a low-order model result in capacitance with an observed effective value significantly larger than the one calculated using only the physical properties of the air. The air thermal capacitance multiplier ranges between 6 and 10 [30]. In this paper, we use $C_T = 8$. Equation (1) in matrix form is:

$$\begin{Bmatrix} T_1 \\ \vdots \\ T_N \end{Bmatrix}^{t+1} = \begin{Bmatrix} \frac{\Delta t}{C_1} \\ \vdots \\ \frac{\Delta t}{C_N} \end{Bmatrix} \odot \left(\begin{bmatrix} -\sum_j^N U_{1j} - \sum_k^M U_{1k} + \frac{C_1}{\Delta t} & U_{12} & \dots & U_{1N} \\ \vdots & \vdots & \ddots & \vdots \\ U_{N1} & U_{N2} & \dots & -\sum_j^N U_{Nj} - \sum_k^M U_{Nk} + \frac{C_N}{\Delta t} \end{bmatrix} \begin{Bmatrix} T_1 \\ \vdots \\ T_N \end{Bmatrix}^t + \begin{Bmatrix} \dot{Q}_1 + \sum_k^M (U_{1kk}T_{kk}) \\ \vdots \\ \dot{Q}_N + \sum_k^M (U_{Nkk}T_{kk}) \end{Bmatrix} \right) \tag{2}$$

where

- $\odot$: is an elementwise multiplication operator.
- N: is the number of nodes.
- M: is the number of nodes with known temperatures.

To assure numerical stability in the solution, the time step must be chosen according to the stability criterion defined in Equation (3):

$$\Delta t \leq min \left(\frac{C_i}{\sum U_i} \right) \tag{3}$$

Using Equation (4), the proportional–integral control (PI controller) calculates the heat produced by the heating system at each time step, and the integral part should be reset periodically.

$$\dot{Q}^{t+1} = k_{\text{p}} \cdot \left(T^t_{\text{setpoint}} - T^t_{\text{room.air}} \right) + k_{\text{i}} \int \left(T^t_{\text{setpoint}} - T^t_{\text{room.air}} \right) dt \tag{4}$$

where

- k_{p}: proportional gain of the controller, W/K.
- k_{i}: integral gain of the controller, W/K·s.

Equation (5) illustrates state-space representations of linear differential equation systems. In this equation, (**x**) is the state vector with n elements, (**u**) is the input vector with p elements, and (**y**) represents output vectors with q elements. The vectors are linked by the following matrices: **A** (n × n), **B** (n × p), **C** (q × n), and **D** (q × p).

$$\dot{\mathbf{x}} = \mathbf{Ax} + \mathbf{Bu} \qquad \mathbf{y} = \mathbf{Cx} + \mathbf{Du} \tag{5}$$

Temperatures of thermal capacitances are generally considered the system's state in this approach since they have specific physical meaning and are relatively easy to measure [26]. Model identification refers to determining the physical properties of unknown systems based on some experimental or training data. In this paper, the Python function SLSQP is used to minimize the coefficient of variance of the root mean square error (CV-RMSE) as a fit metric. In accordance with ASHRAE Guideline 14, the model should not exceed a CV-RMSE of 30% relative to hourly measured data [31]. By minimizing CV-RMSE, the optimization algorithm determines the equivalent parameters for RC circuits. Equation (6) [31] is used to calculate CV-RMSE, where T_i represents the measurement data, $\hat{T}_i$ represents the simulation results, n corresponds to the total number of observations, and $\overline{T}$ represents the average of all measurements.

$$CV - RMSE(\%) = 100 \times \frac{\sqrt{\left[\sum_{i=1}^{n} \left(T_i - \hat{T}_i \right)^2 / n \right]}}{\overline{T}} \tag{6}$$

This methodology can be used to create archetype RC thermal networks for representative zones. For example, Figure 1 presents a third-order thermal network RC model (4R3C) for zones with a convective system, which is defined by three state variables.

The inputs to this RC thermal network model are outdoor temperature (T_{ext}), solar heat gain (Q_{SG}), internal heat gain from occupants and equipment (Q_{IG}), and heat delivered by local water–air heat pumps (Q_{aux}), and the output is the indoor air temperature. Montreal weather data are used to determine the outdoor temperature and solar irradiance [32]. Then, the performance of the RC thermal network model is validated with measured data. Table 1 presents an overview of the third-order thermal network parameters.
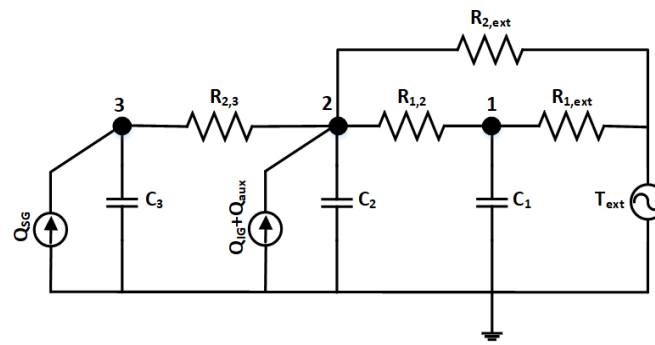
Figure 1. Thermal network model of the zones with convective system.

Table 1. Description of RC thermal network model parameters (4R3C).

Parameter	Description	Parameter	Description
$R_{1,\,ext}$	Resistance of Wall	1	Envelope node
$R_{1,2}$	Resistance between wall and air	2	Indoor air temperature node
$R_{2,3}$	Resistance between floor and air	3	Floor temperature node
$R_{2,\,ext}$	Resistance of infiltration	T_{ext}	Outdoor temperature
C_1	Capacitance of Envelope	Q_{SG}	Solar heat gain
C_2	Capacitance of effective air	Q_{IG}	Internal heat gain
C_3	Capacitance of floor	Q_{aux}	Heating power

2.3. Energy Flexibility Quantification

The term "building energy flexibility" refers to "the ability to deviate from the reference scenario at a specified point in time and for a specified period" [6]. Enhancing energy flexibility is essential for balancing supply and demand on the grid and incorporating renewable energy capacity to reduce peak demand at key periods for the grid. Flexibility is also essential for providing contingency reserves for emergencies (e.g., after a power outage) and enabling dynamic electricity trading. Flexible buildings can also meet immediate or short-term grid needs.

Thus, real-time energy flexibility should be predicted and calculated on short notice (e.g., kilowatts available over the next few hours). This paper presents dynamic building energy flexibility indexes (BEFI) to quantify energy flexibility in school buildings and their interaction with the smart grid. We have described the BEFI concept in two previous conference papers on the topic with a preliminary introduction and case studies [33]. By implementing the flexibility strategy and using the reference as-usual profile, Equation (7) calculates the average $\overline{BEFI}$ at time t for duration Dt, Equation (8) presents the BEFI as a percentage, and Equation (9) quantifies $BEFI\%$ at the building level.

$$\overline{BEFI}(t, Dt) = \frac{\int_t^{t+Dt} P_{\text{ref}} dt - \int_t^{t+Dt} P_{\text{Flex}} dt}{Dt} \tag{7}$$

$$BEFI\% = \frac{P_{\text{ref}} - P_{\text{Flex}}}{P_{\text{ref}}} \tag{8}$$

$$BEFI_{building} = \sum_1^n BEFI_{zone} \tag{9}$$

A model can be used to determine the difference in power demand (*P*, unit: Watt) between the reference case (P_{ref}) and the flexible case (P_{Flex}) to determine the available flexibility. This calculation gives the available flexibility at time t. Every hour, the calculation is repeated to give the available flexibility over the period $\overline{BEFI}(t, Dt)$.

3. Description of the Case Study: Electrically Heated School Building

The case study school (Figure 2) is an electrically heated building located in Sainte-Marthe-sur-le-Lac (near Montreal, QC, Canada). The total floor area of this two-story school building is 5192 m^2 (2596 m^2/story). The school includes the following features:

- In operation since 2017.
- Hydronic radiant floor systems in several zones (gym and offices).
- Convective systems in several zones (classrooms, library, kindergarten).
- A 28-loop geothermal system.
- An Electrically heated Thermal Energy storage device (ThermElect) with an 80 kW heating capacity. ThermElect converts electrical power into stored heat when the price of electricity is low (or when demand on the grid is low) and provides heat when demand is high.
- Water–air Heat pumps with a heating capacity of 40 kW at 36 terminals.
- Water–water heat pump with a capacity of 33 kW.

Figure 2. Electrically heated school building, Horizon-du-Lac (near Montreal, QC, Canada).

The building automation system (BAS) and dedicated electrical submeters at this school provide high-quality data with a sampling timestep of fifteen minutes. The thermocouples are T-types with a standard accuracy of 0.2 °C for the temperature range of 0 to 70 °C. The gym and offices have been designed with significant thermal mass, which helps to improve energy flexibility. Table 2 presents some of the key features of the school building:

Table 2. Key features of the school building.

General Information	
In operation since	2017
Site	Sainte-Marthe-sur-le-Lac, Québec, Canada
Latitude	45.5
ASHRAE climate zone	6
Heating degree days	4495
Net floor area (m^2)	2596 m^2/floor
Number of floors	2
Window type	Double-glazed argon low-e

Table 2. *Cont.*

Mechanical	
Space heating/cooling	Ground-source water–water HP and local water–air HPs
Ventilation system	Balanced mechanical ventilation with DCV, with centralized AHUs with rotary heat recovery. Centralized dedicated outdoor air system (DOAS) modulated based on CO_2
Main system, features	Ground-source heat pump (GSHP), energy recovery ventilator (ERV)
DHW source	Electricity boiler
Electrical	
Lighting, typical type, controls	LED-tube luminaires

System Description

Figure 3 illustrates the schematic of the building's heating system. The system consists of an integrated geothermal system, ThermElect, a water–water heat pump, local water–air HPs, and a hydronic radiant floor system. All heating systems are electrical devices and hence provide a link with the electrical grid. A predictive controller can exploit this link to help balance electricity production and demand, among other potential uses.
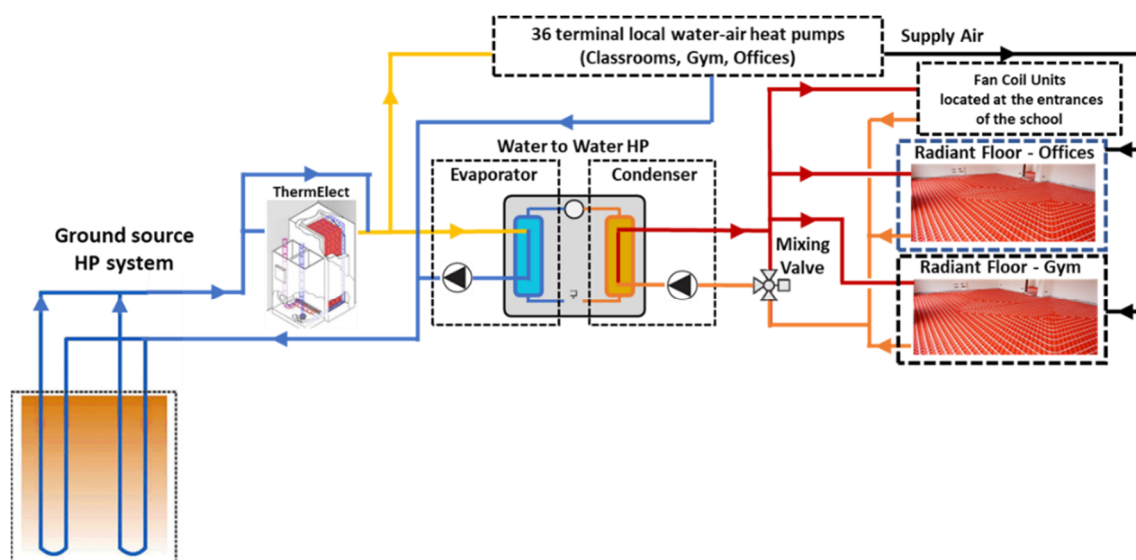
Figure 3. Process flow diagram (PFD) of the building heating systems.

The water–water HP has a capacity of 33 kW in two stages (16.5 kW per stage) and a maximum water supply temperature of 48.8 °C. Borehole Thermal Energy Storage (BTES) with 28 loops on the evaporator side of the HP generates low-temperature heat. A thermal energy storage device (ThermElect) pre-heats the water input to local water–air HPs and water–water HP. The supply water temperature of the HP to the zones is controlled through a thermostatic three-way valve with a maximum temperature setting of 48.8 °C. Thermostats regulate the indoor temperature in each zone separately. The hydronic radiant heating and convective systems supply space heating in the offices and the gym.

4. Modeling Results and Discussion

4.1. Archetype Zones with Convective System: Classrooms

Figure 4 shows one of the classrooms in this school. Classrooms are equipped with ground-source water–air heat pumps (1.5–2 tons each) with COP of 3.2 and proportional–integral control (PI) in the local-loop control of room temperature. The classrooms are

typically 9.1 m long by 7.2 m wide, with ceiling–floor heights of 3.0 m. Figure 5 shows a schematic of a classroom equipped with a water-to-air HP:
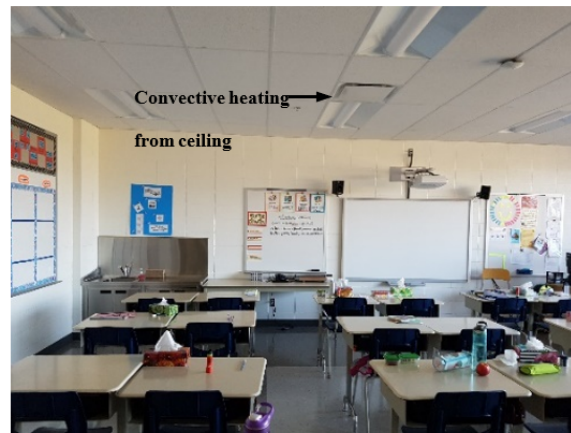

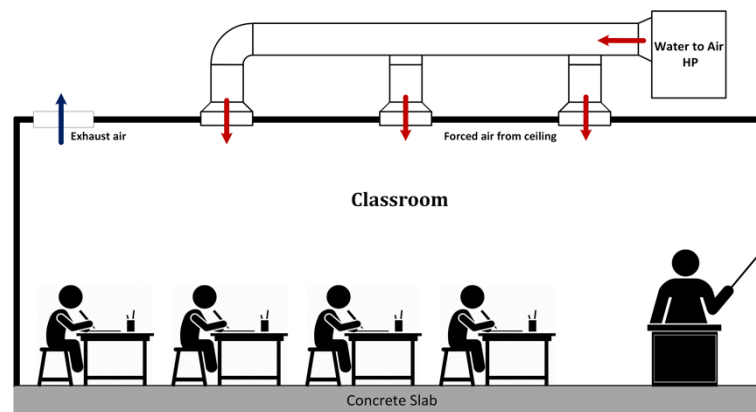**Figure 4.** Typical classroom with convective heating.

Figure 5. Schematic of a classroom with water–air heat pump.

Figure 6 presents the thermal network RC model structures for zones with convective systems. Figure 6a–c shows the first-order model (1R1C), second-order model (3R2C), and third-order model (4R3C), respectively. The inputs for the analyzed models include outdoor temperature (T_{ext}), solar heat gain (Q_{SG}), internal heat gain (Q_{IG}), and heat delivered by water–air heat pumps (Q_{aux}). Montreal weather data are used to determine outdoor temperature and solar radiation. In the measured data, the heat supplied by water–air HP is calculated by multiplying the measured electricity demand by COP of the HP and is used for comparison of models and measurements (shown in Figure 7). The solar heat gains, internal gains, and heating for the third-order model are distributed over the thermal capacitances (Figure 6c). The performance of the simplified RC models from the first-order to the third-order model is validated with measured data, as shown in Figure 7a–c.

As shown in Figure 7a, the first-order model cannot capture the system's dynamics well. The second-order model has better calibration results than the first-order model, but it still cannot capture details of the thermal dynamics of the system (Figure 7b). The calibration of the third-order model (Figure 7c) shows good accuracy and adequate statistical indices (CV-RMSE of 8% and a maximum difference of 0.4 °C). It should be noted that higher-order models require additional inputs, such as heat flux measurements, to guarantee observability. Since these measurements will not be available in most buildings, higher-order models' identity cannot be guaranteed [28].
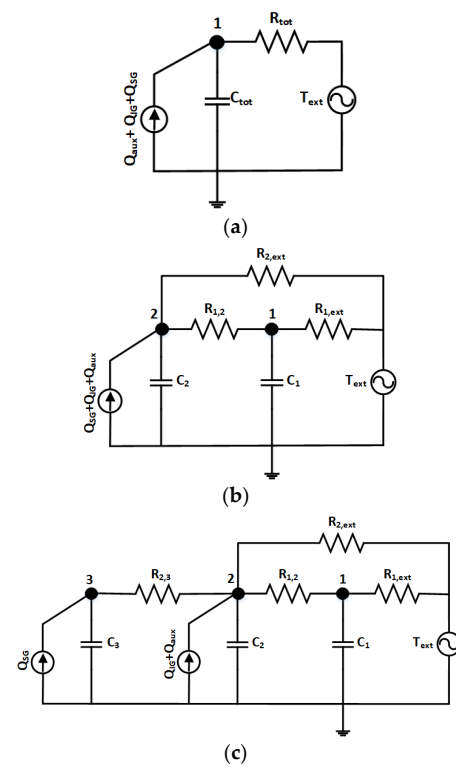
Figure 6. RC thermal network model: (**a**) first-order, (**b**) second-order, and (**c**) third-order models.
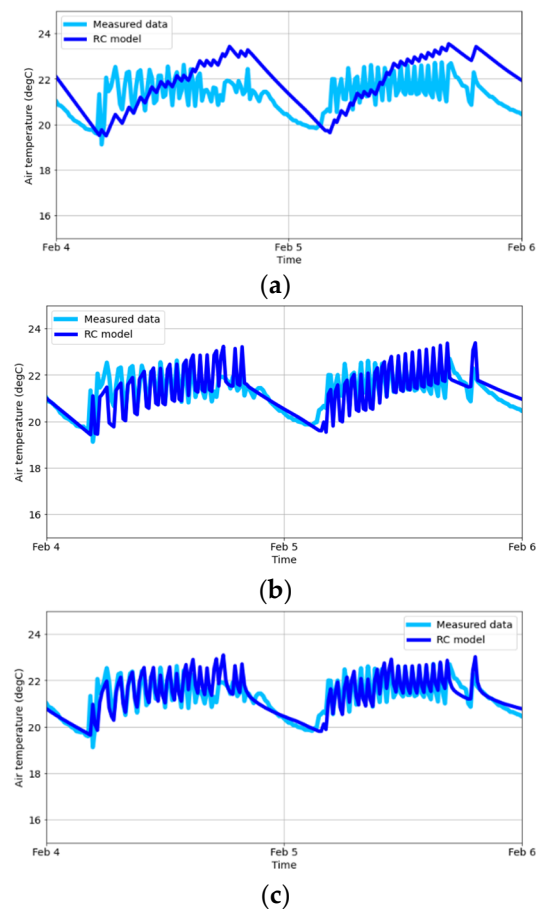

Figure 7. Calibration of RC thermal network models with measured data: (**a**) first-order, (**b**) second-order, and (**c**) third-order models.

4.1.1. Weather Conditions: Cold Winter Days

Weather data for Montreal's coldest days (5–8 February 2020) are selected because peak energy demand occurs under these conditions. Figure 8 presents the outdoor temperature and solar flux during these days. The weather data are measured data and were obtained from the hourly Montreal weather file [32].
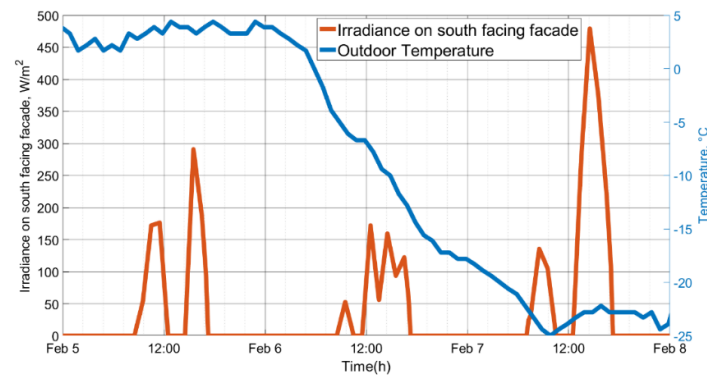
Figure 8. Outdoor temperature and solar flux-Montreal's coldest days.

4.1.2. Available Energy Flexibility in Contingency Event

Contingency reserves are amounts of power that a utility can use in the event of the loss of a generation unit or unexpected load imbalance. To address this need, real-time thermal load flexibility should be predicted ahead of time or calculated continuously and should be available at short notice (e.g., 10 min) over an hour or several hours. This section presents the contingency strategy to quantify the energy flexibility available from the zones with a convective system to the grid at specific times. In this case, a tolerance band setpoint profile is proposed. A flexible approach is proposed within the tolerance limits where the temperature is allowed to deviate from the reference setpoint. For example, during a flexibility event occurring at 2 p.m. for one hour, the temperature is allowed to drop by 2 degrees to provide a "temporary relief" to the heating system (Figure 9a). At this point, the setpoint is lowered two degrees (from 24 to 22 °C). Figure 9b shows the results of available energy flexibility during contingency events.
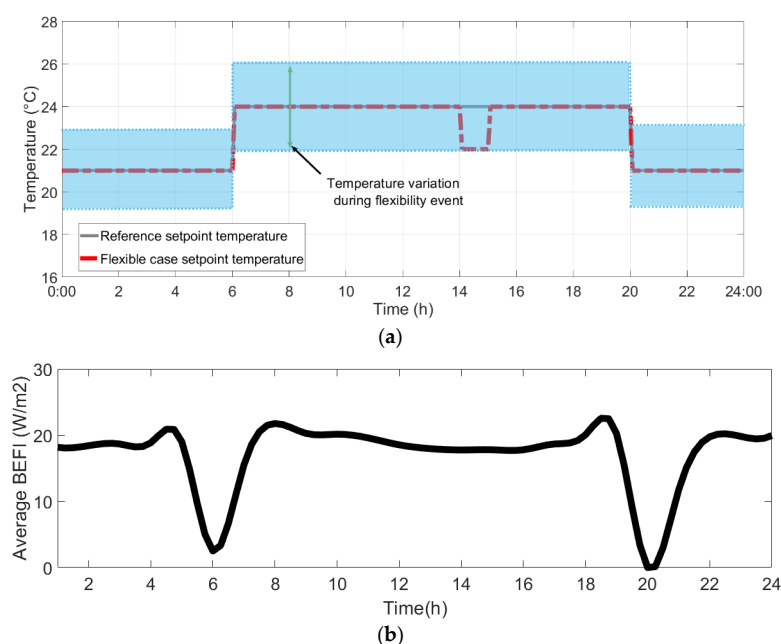

(**a**)

(**b**)

Figure 9. (**a**) Daily setpoint profile with acceptable temperature band and a flexibility event with a duration of 1 h at 2 pm; (**b**) energy flexibility curve, 1 h event.

According to Figure 9b, energy flexibility of around 20 W/m^2 can be provided to the grid in the event of loss of a generation unit or other unexpected power outages. The BEFI can be implemented in the BAS with a predictive model controller, which can optimize power flexibility for a known period of high demand. This makes BEFI appropriate for various grid requirements, including contingency reserves and load shifting.

4.2. Archetype Zones with Hydronic Radiant Floor and Convective Heating Systems

Figure 10 presents a schematic of the office zones equipped with local water–air HP and a hydronic radiant floor system on the school's first floor.
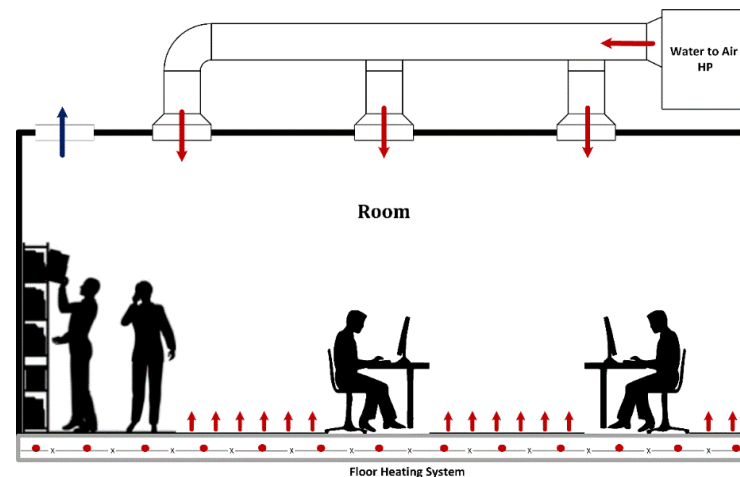
Figure 10. Schematic of the office zone equipped with hydronic radiant floor and convective systems.

The plan view of the offices and piping of the hydronic radiant floor system is shown in Figure 11. These offices are heated with hydronic radiant and local convective systems. Proportional–integral thermostats control heating systems. The thermocouples in the offices are T-types with a standard accuracy of 0.2 °C for the temperature range of 0 to 70 °C. In addition to air temperatures, floor temperatures are also measured at eight different locations, as shown in Figure 11.
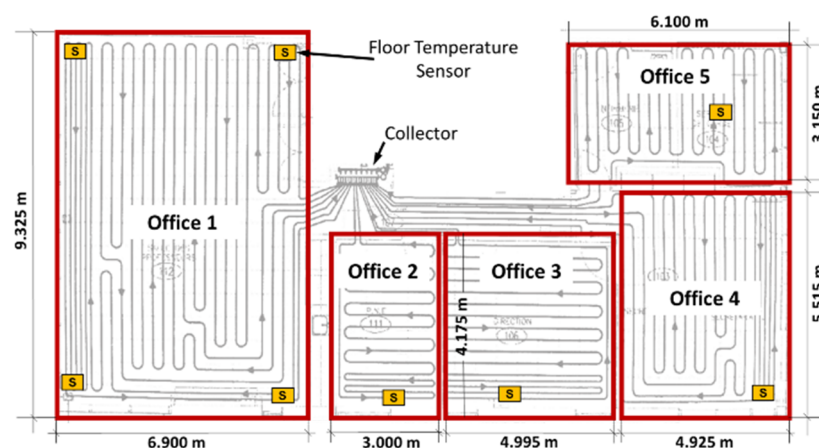

Figure 11. Plan view of the offices with hydronic radiant floor system.

Table 3 presents the radiant hydronic floor area in each zone and the piping length.

Table 3. Floor area and piping length of the offices with hydronic radiant system.

Thermal Zone	Area (m^2)	Piping Length (m)
Office 1	64	244
Office 2	12	69
Office 3	21	91
Office 4	27	176
Office 5	19	87
Total	143	667

A front view of the slab with hydronic radiant piping can be seen in Figure 12. The floor is a concrete slab 15 cm thick insulated at the bottom with total thermal resistance of 5.64 m^2 K/W. The pipe is made of cross-linked polyethylene (PEX), has a diameter of 1.25 cm, and is located at the depth of 6 cm. The pipes were kept in place by a wire mesh before casting concrete, and the distance between the pipes was 30.4 cm.
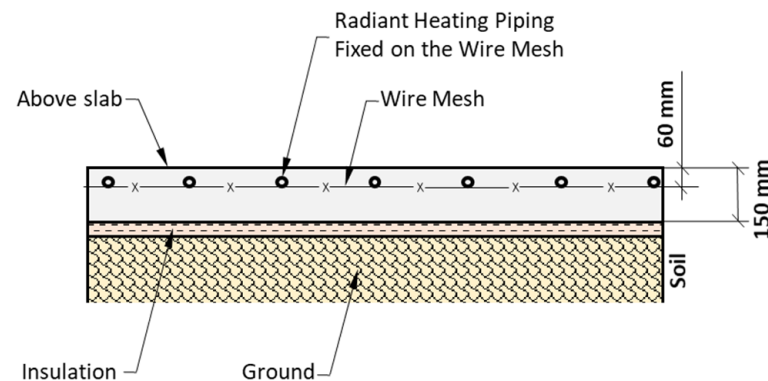
Figure 12. Slab cut with hydronic radiant heating piping.

Concrete's properties are affected by its age, temperature, humidity, and moisture content [34]. Following ASHRAE [35], a normal-density concrete has a conductivity of 1.7 W/(m·K), specific heat of 800 J/(kg·K), and a density of 2200 kg/m^3. A water–water HP provides a controlled flow rate of 0.29 L/s with a maximum temperature of 48.8 °C. The HP has a nominal COP of 2.7 under full load conditions at 48.8 °C. Heating power to the hydronic radiant system is calculated by Equation (10):

$$Q = \dot{m} \times c_p \times \Delta T \tag{10}$$

According to the ASHRAE standard 55, the floor temperature must not exceed 29 °C [36]. Thus, a floor surface temperature of 26 °C is considered in this study. Several floor sensors and control valves protect the floor from overheating and enhance thermal comfort. The RC thermal network for the zones with hydronic radiant and convective heating/cooling systems is shown in Figure 13. The inputs are outdoor temperature (T_{ext}), solar gain (Q_{SG}), internal heat gain (Q_{IG}), heat delivered by the hydronic radiant system (q_{RF}), and heat delivered by the convective system (Q_{aux}). These inputs can be:

- *Controllable:* such as the heat delivered by the heating systems and the ventilation airflow rate.
- *Uncontrollable:* such as the outdoor temperature, solar gains, and internal gains.
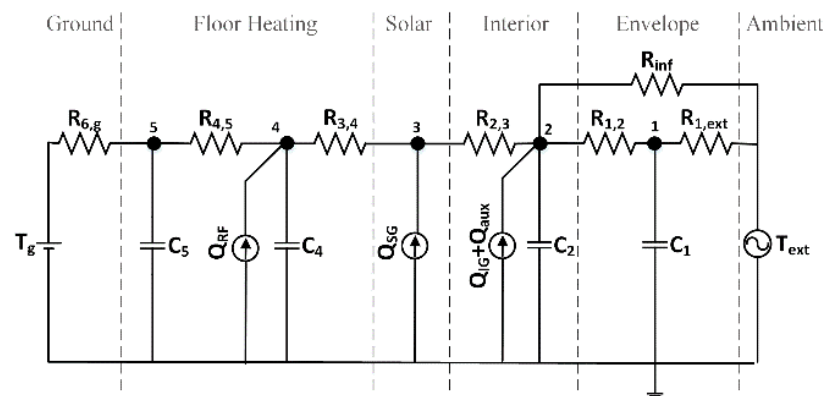
Figure 13. RC thermal network model of the zones with hydronic radiant floor system and convective system.

The performance of the simplified RC model is validated with measured data, as shown in Figure 14.
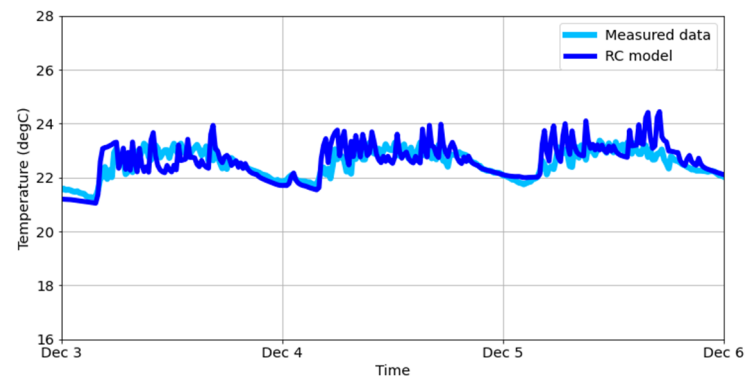

Figure 14. Calibration of RC thermal network model with measured data, zones with hydronic radiant floor system and convective system.

Table 4 provides an overview of the thermal network model parameters:

Table 4. Description of RC thermal network model parameters (7R4C).

Parameter	Description	Parameter	Description
1	Node of envelope	$R_{1,ext}$	Resistance of wall, (K/W)
2	Node of indoor air	$R_{1,2}$	Resistance between wall and air node, (K/W)
3	Node of floor surface	$R_{2,3}$	Resistance between floor and air node, (K/W)
4	Node of pipe	R_{inf}	Resistance of infiltration, (K/W)
5	Node of concrete (top)	$R_{3,4}$	Resistance between pipe and floor surface, (K/W)
T_{ext}	Temperature of outdoor, (°C)	$R_{4,5}$	Resistance between concrete and pipe, (K/W)
T_g	Temperature of ground, (°C)	$R_{6,g}$	Resistance between ground and concrete, (K/W)
Q_{SG}	Solar heat gain, (W)	C_1	Capacitance of envelope, (J/K)
Q_{IG}	Internal heat gain, (W)	C_2	Capacitance of effective Air, (J/K)
Q_{aux}	Heating power, (W)	C_4	Capacitance of floor (top), (J/K)
Q_{RF}	Heating of radiant floor, (W)	C_5	Capacitance of floor (below), (J/K)

4.2.1. Control Scenarios for Energy Flexibility Activation in Archetype Zones with Hydronic Radiant Floor and Convective Systems

This section investigates the heat supplied to the zones with hydronic radiant and convective systems. It will be possible to develop simple predictive control strategies that use thermal storage potential while also considering peak load and thermal comfort. In the reference case (a business-as-usual case), the hydronic radiant floor temperature setpoint (21.8 °C) is always lower than the air temperature setpoint (23 °C) during the daytime (Figure 15a). As a result, the convective system is the primary heating system, and the floor acts as a heat sink. In this study, alternative control scenarios for a cold winter day are examined and compared to current building operations as a reference case. Assumptions considered in designing control strategies include:

- To maintain the slab temperature within the comfort range, the slab surface is set to a maximum of 26 °C.
- The water–water HP can deliver up to 15 kW of heat to the radiant floor heating system, according to the observation from measured data.
- The operating temperature is considered to be the effective indoor temperature.
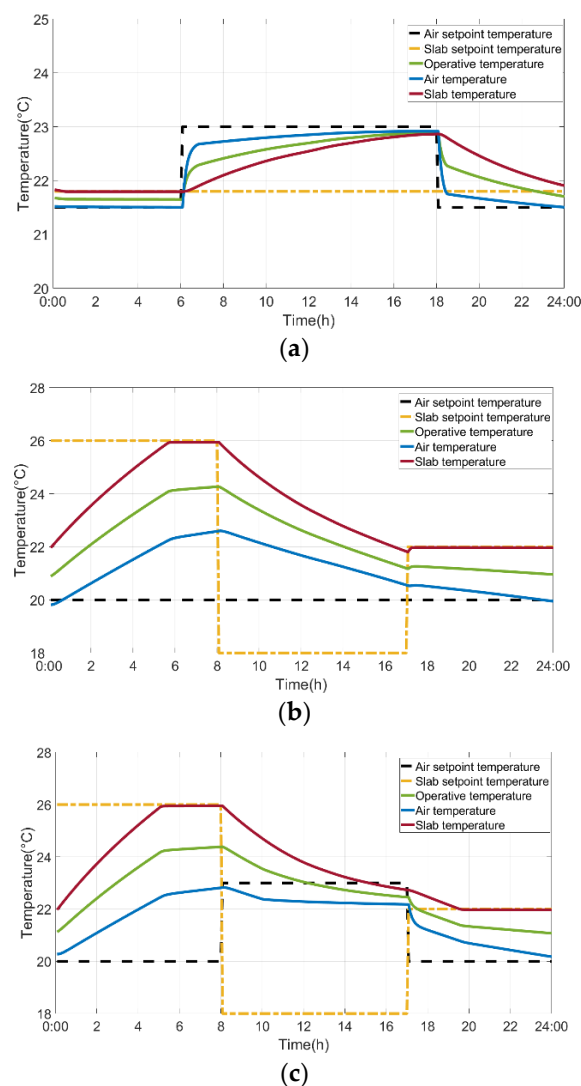- During unoccupied hours (nighttime), the slab is charged and discharged during occupied hours (daytime).

(a)

(b)

(c)

Figure 15. Temperature profile in different control strategies: (**a**) Control Strategy 1 (reference case); (**b**) Control Strategy 2; (**c**) Control Strategy 3.

1. Control Scenario 1 (Reference Case)

The reference case is presented in Figure 15a, which is the current operation of zones with hydronic radiant heating. In this scenario, the convective system is the primary heating system, and the hydronic radiant system is not commonly used. As seen in Figure 16a, in this case, the peak load is 10 kW and occurs during the on-peak hours (6 a.m. to 9 a.m.). Thus, in order to improve the energy flexibility of the building, the following two control scenarios are presented.

(a)

(b)

(c)
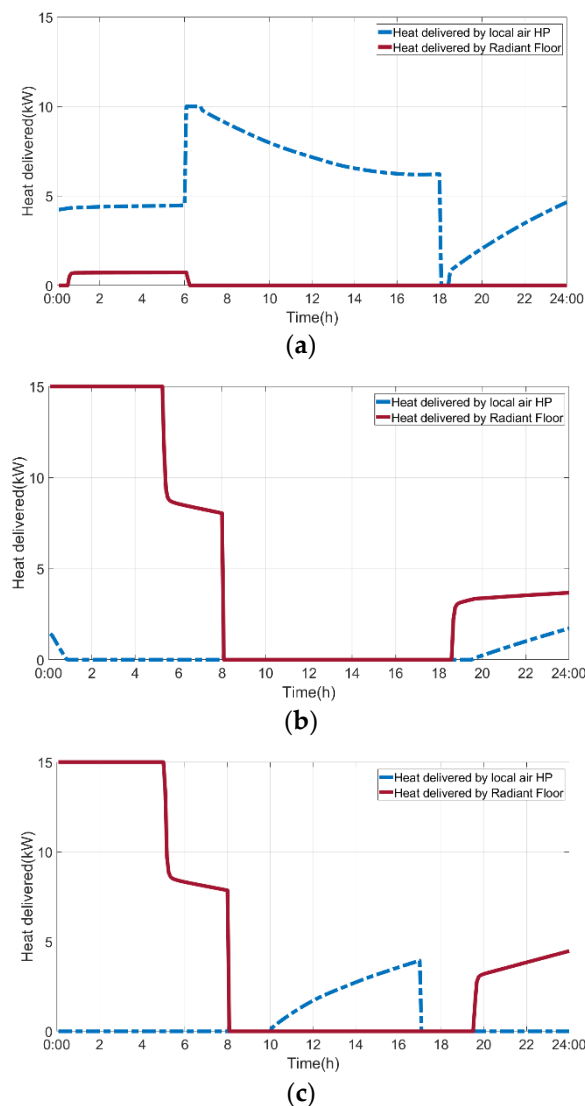
Figure 16. Heat delivered to the thermal zones in different control strategies: (**a**) Control Strategy 1 (reference case); (**b**) Control Strategy 2; (**c**) Control Strategy 3.

2. Control Scenario 2 (Constant Air Setpoint Temperature)

This control scenario involves preheating the slab from midnight to 8:00 a.m. with a setpoint temperature of 26 °C (Figure 15b). During occupied hours (from 8:00 a.m. to 5:00 p.m.), the slab's set point temperature is 18 °C, and then it is raised to 22 °C. It is considered that the air setpoint temperature is always constant and equal to 20 °C during occupied and non-occupied hours.

According to Figure 15b, the operative temperature varies between 21 and 24 °C, which is within the thermal comfort range for the occupants. In Figure 16b, the heat delivered to the thermal zones is calculated using Control Scenario 2. In this control scenario, the radiant

floor system is the primary heating system, and the heating demand during occupied hours is reduced. It should be noted that in this control scenario, the ventilation system is off, resulting in poor air quality in the offices. Therefore, Control Strategy 3 is presented to address the air quality of the zones during occupied hours.

3.   Control Scenario 3 (Variable Air Setpoint Temperature)

As part of this control scenario, the air setpoint temperature is increased to 23 °C during occupied hours (Figure 15c). As a result, the morning peak load can be reduced, and fresh air can be provided to the zones from 10:00 a.m. to 5:00 p.m. The energy consumption in this flexible scenario is 133.5 kWh, which is less than the reference case (136.6 kWh). The following section will address the slab's state of charge (SOC) (i.e., thermal storage), as well as the flexibility associated with reducing peak loads and energy consumption over peak periods.

4.2.2. State of Charge (SOC) of the Slab

The thermal inertia in the slab can provide the flexibility to reduce peak loads and shift the heat production of the radiant heating system in time. State of charge (SOC) is a concept that describes how much energy is stored at time t relative to the total capacity, as shown in Equation (11) [37]:

$$SOC = \frac{E_{th}(t) - E_{th,min}(t)}{E_{th,max}(t) - E_{th,min}(t)} \tag{11}$$

The *SOC* is the percentage of the stored thermal energy as a function of the minimum and maximum slab surface temperatures, as given by [38].

$$SOC = \frac{T_{\mathrm{slab}}(t) - T_{\mathrm{th,min}}(t)}{T_{\mathrm{th,max}}(t) - T_{\mathrm{th,min}}(t)} \tag{12}$$

where $T_{\mathrm{th,max}}$ is the maximum slab surface temperature, set at 26 °C for indoor thermal comfort, and $T_{\mathrm{th,min}}$ is the minimum slab surface temperature, considered equal to the average indoor air temperature.

Figures 17 and 18 illustrate heat storage and SOC of the slab in the reference case (Control Strategy 1) and flexible case (Control Strategy 3). It can be observed that in the reference case, the slab cannot be fully charged. Thus, the thermal energy storage capacity of the slab is not fully utilized; while using a flexible case (Control Strategy 3), the slab is fully charged during unoccupied hours and discharged during on-peak hours. This approach activates the thermal load flexibility of the school and allows the electricity grid to manage electricity demand when needed.
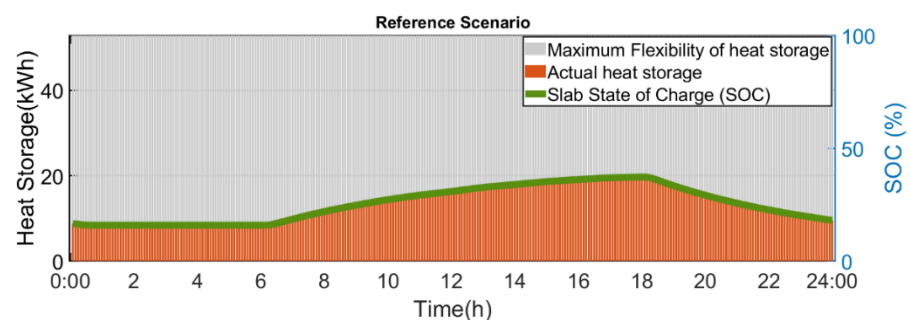

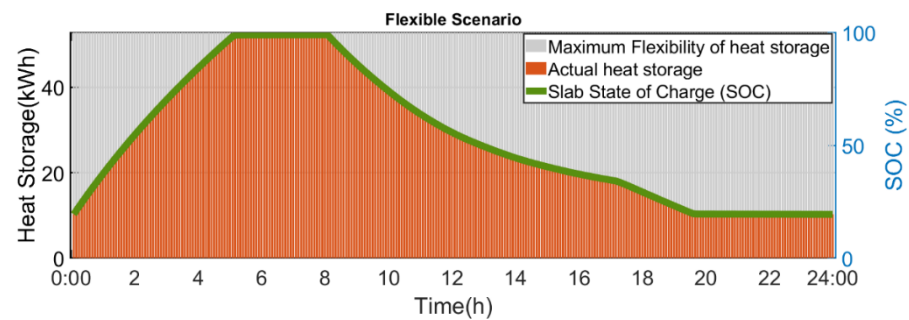**Figure 17.** Heat storage and state of charge (SOC) of the slab (reference case).

Figure 18. Heat storage and state of charge (SOC) of the slab (flexible case).

4.2.3. Thermal Load Flexibility in Archetype Zones with Hydronic Radiant System

Equations (7)–(9) calculate BEFI by implementing the flexibility strategy and comparing it with the reference as-usual profile. In Figure 19, a flexibility strategy is applied to zones with hydronic radiant and convective heating systems to calculate the hourly BEFI.
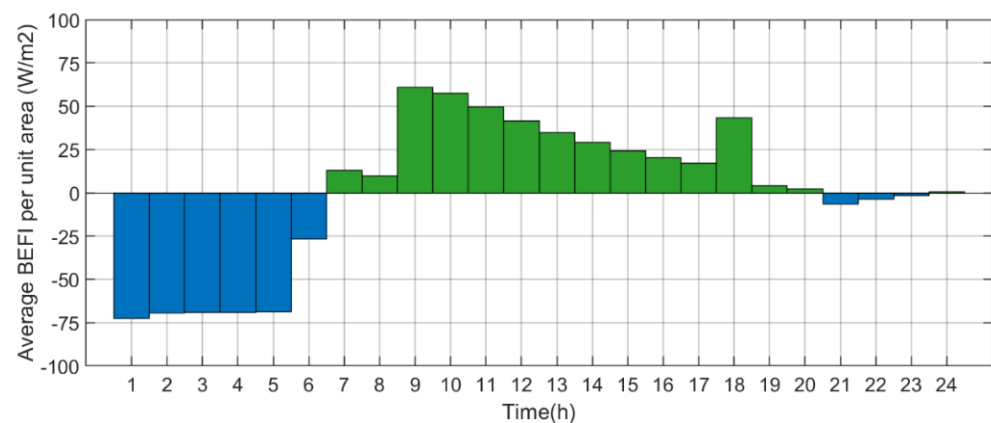

Figure 19. Average hourly BEFI (flexible control strategy).

By applying a flexible control strategy, available hourly BEFI provided to the grid during on-peak hours is positive, indicating the power reduction value available compared to the reference case. During nighttime (off-peak hours), the BEFI is negative, showing a higher power demand for charging the slab and preheating the zones. Based on Figure 19, around 60 W/m^2 energy flexibility can be provided to the grid in the morning and 45 W/m^2 in the evening (on-peak hours).

4.3. Building Level Energy Flexibility

Figure 20 presents energy flexibility at the building level. Zones with radiant floor and convective heating systems can provide around 60 W/m^2 energy flexibility. Additionally, classrooms and the library with convective heating systems can provide 20 W/m^2 during on-peak hours. In total, by implementing appropriate control strategies, the school building can provide energy flexibility from between 30 W/m^2 and 80 W/m^2 when needed by the grid.

In this school, the gym and offices' floor area is 586 m^2, and the classrooms', libraries', and kindergartens' floor is 2054 m^2. Therefore, the school at the building level has potential flexibility of between 50 and 80 kW, representing 40 to 65% building energy flexibility. This bottom-up approach opens the path towards labeling energy flexibility in school buildings as part of the future smart grid and smart cities.
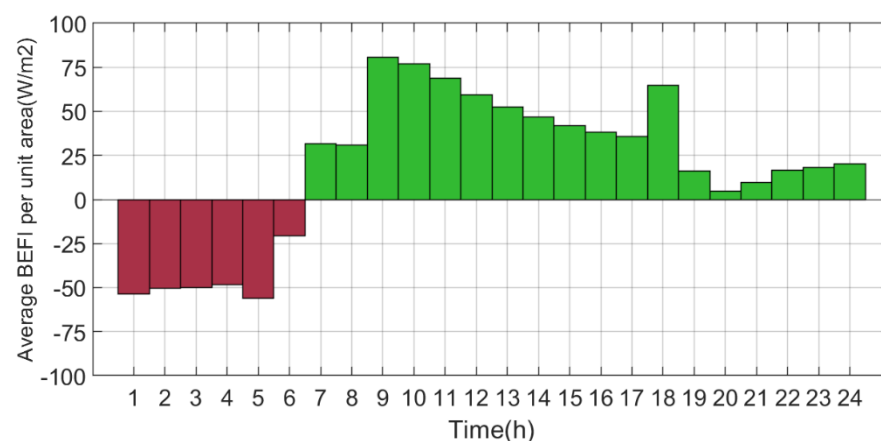
Figure 20. Hourly building energy flexibility in school.

5. Conclusions

School buildings are an important part of the building stock; they also represent a sizable portion of the total energy use in the building sector. Therefore, quantification of energy flexibility in school buildings has a significant role in providing a safe and efficient operation of the future resilient grid. This paper presented a practical methodology that facilitates the modeling and implementation of appropriate control strategies in school buildings. This paper also presented a methodology for defining and calculating a dynamic energy flexibility index for buildings. The dynamic building energy flexibility index (BEFI) is defined in terms of key performance indicators relative to a reference energy consumption profile at the zone level, building level, and as a percentage. The application of the BEFI was presented for an electrically heated school building in Canada. This study illustrated how low-order lumped parameter thermal network models could be utilized to calculate the BEFI. Furthermore, the activation of energy flexibility through a rule-based approach with near-optimal setpoint profiles is investigated. Results show that applying appropriate control strategies can enhance the school building energy flexibility by 40% to 65% during peak demand periods. In addition to improving energy flexibility in school buildings, these control strategies could reduce the size of HVAC units at the design stage, thereby lowering their operating and initial capital costs.

Conflicts of Interest: The authors declare no conflict of interest.

Abbreviations

BAS	Building automation system
BEFI	Building energy flexibility index (W)
BTES	Borehole thermal energy storage
C	Thermal capacitance (J/K)
COP	Coefficient of performance
CV-RMSE	Coefficient of variance of the root mean square error
DSM	Demand-side management
Dt	Time (seconds/hours)
EUI	Energy use intensity (kWh/m^2/year)
HVAC	Heating, ventilation, and air conditioning
KPI	Key performance indicator
NZEB	Net zero energy building
P	Electric power (W)
PV	Photovoltaic
Q_{SG}	Solar gain (W)
Q_{IG}	Internal heat gain (W)
Q_{aux}	Heating power (W)
R	Thermal resistance (K/W)
RES	Renewable energy sources
RC	Resistance–capacitance
SOC	State of charge
T	Temperature (°C)
T_o	Outdoor temperature (°C)
T_{SP}	Setpoint temperature (°C)
Subscripts	
Flex	Flexible case
Ref	Reference case
SP	Setpoint

References

1. Davito, B.; Tai, H.; Uhlaner, R. The smart grid and the promise of demand-side management. *McKinsey Smart Grid* **2010**, *3*, 8–44.
2. Foteinaki, K.; Li, R.; Heller, A.; Rode, C. Heating system energy flexibility of low-energy residential buildings. *Energy Build.* **2018**, *180*, 95–108. [CrossRef]
3. Weiß, T.; Fulterer, A.M.; Knotzer, A. Energy flexibility of domestic thermal loads—A building typology approach of the residential building stock in Austria. *Adv. Build. Energy Res.* **2019**, *13*, 122–137. [CrossRef]
4. Afram, A.; Janabi-Sharifi, F. Theory and applications of HVAC control systems–A review of model predictive control (MPC). *Build. Environ.* **2014**, *72*, 343–355. [CrossRef]
5. Jensen, S.Ø.; Marszal-Pomianowska, A.; Lollini, R.; Pasut, W.; Knotzer, A.; Engelmann, P.; Stafford, A.; Reynders, G. IEA EBC annex 67 energy flexible buildings. *Energy Build.* **2017**, *155*, 25–34. [CrossRef]
6. Torres Ruilova, B. Evaluation of Energy Flexibility of Buildings Using Structural Thermal Mass. Master's Thesis, Universitat de Barcelona, Barcelona, Spain, 2017.
7. Ilic, D.; Da Silva, P.G.; Karnouskos, S.; Griesemer, M. An energy market for trading electricity in smart grid neighbourhoods. In Proceedings of the 2012 6th IEEE International Conference on Digital Ecosystems and Technologies (DEST), Campione d'Italia, Italy, 18–20 June 2012; pp. 1–6.
8. Lopes, R.A.; Chambel, A.; Neves, J.; Aelenei, D.; Martins, J. A literature review of methodologies used to assess the energy flexibility of buildings. *Energy Procedia* **2016**, *91*, 1053–1058. [CrossRef]
9. Reynders, G. Quantifying the Impact of Building Design on the Potential of Structural Storage for Active Demand Response in Residential Buildings. Ph.D. Thesis, KU Leuven, Heverlee, Belgium, 2015.
10. Afroz, Z.; Shafiullah, G.; Urmee, T.; Higgins, G. Modeling techniques used in building HVAC control systems: A review. *Renew. Sustain. Energy Rev.* **2018**, *83*, 64–84. [CrossRef]
11. Tabares-Velasco, P.; Christensen, C.; Bianchi, M. Simulated peak reduction and energy savings of residential building envelope with phase change materials. *ASHRAE Trans.* **2012**, *118*, 90–97.

12. Morovat, N.; Athienitis, A.K.; Candanedo, J.A.; Dermardiros, V. Simulation and performance analysis of an active PCM-heat exchanger intended for building operation optimization. *Energy Build.* **2019**, *199*, 47–61. [CrossRef]

13. Klein, K.; Herkel, S.; Henning, H.-M.; Felsmann, C. Load shifting using the heating and cooling system of an office building: Quantitative potential evaluation for different flexibility and storage options. *Appl. Energy* **2017**, *203*, 917–937. [CrossRef]

14. Finck, C.; Li, R.; Zeiler, W. Optimal control of demand flexibility under real-time pricing for heating systems in buildings: A real-life demonstration. *Appl. Energy* **2020**, *263*, 114671. [CrossRef]

15. Junker, R.G.; Azar, A.G.; Lopes, R.A.; Lindberg, K.B.; Reynders, G.; Relan, R.; Madsen, H. Characterizing the energy flexibility of buildings and districts. *Appl. Energy* **2018**, *225*, 175–182. [CrossRef]

16. De Coninck, R.; Helsen, L. Quantification of flexibility in buildings by cost curves–Methodology and application. *Appl. Energy* **2016**, *162*, 653–665. [CrossRef]

17. Tumminia, G.; Sergi, F.; Aloisio, D.; Longo, S.; Cusenza, M.A.; Guarino, F.; Cellura, S.; Ferraro, M. Towards an integrated design of renewable electricity generation and storage systems for NZEB use: A parametric analysis. *J. Build. Eng.* **2021**, *44*, 103288. [CrossRef]

18. Ashrae, A.S. *Standard 90.1-2016*; Energy Standard for Buildings Except Low Rise Residential Buildings. American Society of Heating, Refrigerating and Air-Conditioning Engineers, Inc.: Atlanta, GA, USA, 2016.

19. Distribution., H.-Q. État D'Avancement 2012 du Plan D'Approvisionnement 2011–2020. 2012. Available online: http://www.regie-energie.qc.ca/audiences/TermElecDistrPlansAppro_Suivis.html (accessed on 12 January 2022).

20. Hydro-Québec, A.r. Voir Grand Avec Notre Énergie Propre. 2019. Available online: http://www.hydroquebec.com/data/documents-donnees/pdf/rapport-annuel.pdf (accessed on 25 August 2021).

21. Statistic Canada. Elementary–Secondary Education Survey for Canada, the Provinces and Territories. 2017. Available online: https://www150.statcan.gc.ca/n1/dailyquotidien/171103/dq171103c-eng.htm (accessed on 6 November 2020).

22. Issa, M.H.; Attalla, M.; Rankin, J.H.; Christian, A.J. Energy consumption in conventional, energy-retrofitted and green LEED Toronto schools. *Constr. Manag. Econ.* **2011**, *29*, 383–395. [CrossRef]

23. Ouf, M.; Issa, M.; Merkel, P. Analysis of real-time electricity consumption in Canadian school buildings. *Energy Build.* **2016**, *128*, 530–539. [CrossRef]

24. O'Connell, S.; Reynders, G.; Seri, F.; Keane, M. Validation of a Flexibility Assessment Methodology for Demand Response in Buildings. In *IOP Conference Series: Earth and Environmental Science*; IOP Publishing: Bristol, UK, 2019; p. 012014.

25. Gouda, M.; Danaher, S.; Underwood, C. Building thermal model reduction using nonlinear constrained optimization. *Build. Environ.* **2002**, *37*, 1255–1265. [CrossRef]

26. Candanedo, J.A.; Dehkordi, V.R.; Lopez, P. A control-oriented simplified building modelling strategy. In Proceedings of the 13th Conference of International Building Performance Simulation Association, Chambéry, France, 26–28 August 2013.

27. Bacher, P.; Madsen, H. Identifying suitable models for the heat dynamics of buildings. *Energy Build.* **2011**, *43*, 1511–1522. [CrossRef]

28. Reynders, G.; Diriken, J.; Saelens, D. Quality of grey-box models and identified parameters as function of the accuracy of input and observation signals. *Energy Build.* **2014**, *82*, 263–274. [CrossRef]

29. Athienitis, A.; Santamouris, M. *Thermal Analysis and Design of Passive Solar Buildings*; Routledge: London, UK, 2002.

30. Hong, T.; Lee, S.H. Integrating physics-based models with sensor data: An inverse modeling approach. *Build. Environ.* **2019**, *154*, 23–31. [CrossRef]

31. ASHRAE Guideline. *Guideline 14-2002, Measurement of Energy and Demand Saving*; American Society of Heating, Ventilating, and Air Conditioning Engineers: Atlanta, GA, USA, 2002.

32. Hydro-Québec. Simulation Énergétique des Bâtiments. Available online: https://www.simeb.ca:8443/index_fr.jsp (accessed on 12 October 2021).

33. Athienitis, A.K.; Dumont, E.; Morovat, N.; Lavigne, K.; Date, J. Development of a dynamic energy flexibility index for buildings and their interaction with smart grids. In Proceedings of the 2020 Summer Study on Energy Efficiency in Buildings, Virtual, 17–21 August 2020.

34. Marshall, A. The thermal properties of concrete. *Build. Sci.* **1972**, *7*, 167–174. [CrossRef]

35. Ashrae, I. *2009 ASHRAE Handbook: Fundamentals*; American Society of Heating, Refrigeration and Air-Conditioning Engineers: Atlanta, GA, USA, 2009.

36. *ASHRAE 55*; Thermal Environmental Conditions for Human Occupancy. American Society of Heating, Refrigeration and Air-Conditioning Engineers: Atlanta, GA, USA, 2017.

37. Reynders, G.; Lopes, R.A.; Marszal-Pomianowska, A.; Aelenei, D.; Martins, J.; Saelens, D. Energy flexible buildings: An evaluation of definitions and quantification methodologies applied to thermal storage. *Energy Build.* **2018**, *166*, 372–390. [CrossRef]

38. Gouvernement du Québec. *Plan Directeur en Transition, Innovation et Efficacit Energetiques du Quebec 2018–2023*; Gouvernement du Québec: Québec City, QC, Canada, 2018.